Eur. Phys. J. A (2017) **53**: 216
DOI 10.1140/epja/i2017-12412-5

THE EUROPEAN PHYSICAL JOURNAL A

Regular Article – Experimental Physics

# Conversion-electron spectroscopy and gamma-gamma angular correlation measurements in $^{116}$Sn

D.S. Cross[1,a], J.L. Pore[1,b], C. Andreoiu[1], G.C. Ball[2], P.C. Bender[2,c], A.S. Chester[1], R. Churchman[2], G.A. Demand[3], A. Diaz Varela[3], R. Dunlop[3], A.B. Garnsworthy[2], P.E. Garrett[3], G. Hackman[2], B. Hadinia[3], B. Jigmeddorj[3], A.T. Laffoley[3], A. Liblong[3], R. Kanungo[4], D.T. Miller[2,d], B. Noakes[1], C.M. Petrache[5], K. Starosta[1], C.E. Svensson[3], P. Voss[1,e], Z-M. Wang[1,2], J.M. Wilson[3], J.L. Wood[6], and S.W. Yates[7]

[1] Department of Chemistry, Simon Fraser University, 8888 University Drive, Burnaby BC, V5A 1S6, Canada
[2] TRIUMF, 4004 Wesbrook Mall, Vancouver BC, V6T 2A3, Canada
[3] Department of Physics, University of Guelph, 50 Stone Road E., Guelph ON, N1G 2W1, Canada
[4] Department of Astronomy and Physics, Saint Mary's University, 923 Robie Street, Halifax NS, B3H 3C3, Canada
[5] CSNSM, CNRS-IN2P3, Université Paris-Saclay, 91405 Orsay Cedex, France
[6] School of Physics, Georgia Institute of Technology, 837 State Street, Atlanta GA, 30332-0430, USA
[7] Departments of Chemistry and Physics & Astronomy, University of Kentucky, Lexington KY, 40506-0055, USA

Received: 28 August 2017 / Revised: 6 October 2017
Published online: 20 November 2017 – 
Communicated by A. Gade

**Abstract.** The $^{116}$Sn nucleus was studied via the $\beta^-$ decay of $^{116}$In utilizing the $8\pi$ spectrometer and its auxiliary detectors at TRIUMF-ISAC. The resulting K-shell conversion coefficients, K/L ratios, and multipole mixing ratios are presented. The $2_3^+ \rightarrow 2_1^+ 931\,\text{keV}$ and $2_2^+ \rightarrow 2_1^+ 819\,\text{keV}$ transition mixing ratios were re-measured and found to be $\delta = +1.8^{+0.7}_{-0.5}$ and $-1.83(8)$, respectively. Newly measured mixing ratios for transitions among the low-lying $I^\pi = 4^+$ states in $^{116}$Sn, when combined with $\gamma$-ray intensity data, suggest that the 2529 keV $4_2^+$ state possesses a neutron broken-pair admixture in addition to its dominant proton 2p-2h component.

## 1 Introduction

The nucleus $^{116}$Sn has a major proton shell closure at $Z = 50$, and with 66 neutrons it is situated at the midpoint between the two major shell closures $N = 50$ and $N = 82$. Several decades of experimental studies of this semi-magic spherical nucleus [1] have uncovered an interplay of single-particle and collective effects that manifests as a complex structure of low-lying states.

Probing the structure of these states has been the focus of ongoing experimental work using a variety of methods, including decay spectroscopy [2–4], fusion evaporation [5, 6], scattering experiments [7] and transfer reactions [8–10]. As well, there have been several theoretical studies, among them refs. [11,12]. However, information about the character of the $4^+$ states in $^{116}$Sn is currently limited because spectroscopic information, such as mixing ratios ($\delta$) and level half-lives ($t_{1/2}$), either have large uncertainties or have not been measured. The present work aims to fill this gap through measuring multipole mixing ratios and augmenting them with conversion-electron spectroscopy measurements.

High statistics $\beta$-decay experiments, using a dedicated $\gamma$-ray spectrometer coupled to auxiliary detectors, are ideal for measuring mixing ratios and internal conversion coefficients. When combined with high ion production rates of near-stable parent nuclei, the required high statistics to probe weak transitions in the daughter nuclei can be obtained.

In the present $\beta$-decay study of $^{116}$In, new measurements of mixing ratios for transitions among the low-lying $4^+$ states and remeasurements of mixing ratios between $2^+$ states in $^{116}$Sn were performed. Additionally, K-shell internal conversion coefficients and K/L ratios have been obtained. The $E2/M1$ mixing ratio of the $4_2^+ \rightarrow 4_1^+$ 138 keV transition was measured and combined with its K-shell conversion coefficient to obtain the magnitude of its $E0$

[a] e-mail: dcrossa@sfu.ca
[b] *Present Address*: LBNL, 1 Cyclotron Road, Berkeley CA, 94720, USA.
[c] *Present address*: NSCL, 640 S Shaw Ln, East Lansing MI, 48824, USA.
[d] *Present address*: Idaho National Laboratory, 1955 N Fremont Ave, Idaho Falls ID, 83415, USA.
[e] *Present address*: Department of Physics, Albion College, Albion MI, 49224, USA.

component, which is relevant to the mixing between these states. In combination with $\gamma$-ray intensity data, the measured mixing ratios were used to deduce relative $E2$ and $M1$ strengths in order to characterize the $4^+_{1-5}$ states in terms of their predominant proton or neutron content.

## 2 Experiment

A high-statistics measurement of the $\beta^-$ decay of $^{116}$In to $^{116}$Sn was conducted at TRIUMF-ISAC with the $8\pi$ spectrometer and its suite of auxiliary detectors. A 70 $\mu$A 500 MeV proton beam from the TRIUMF driver cyclotron bombarded a high-power Ta target, generating radioactive atoms which diffused to the surface of the target foils. These atoms were ionized with a Re surface-ion source and then guided through a high-resolution mass separator set to transmit singly-charged $A = 116$ ions. A beam of predominantly $^{116m1}$In ($I^\pi = 5^+$, $t_{1/2} = 54.29$ min) at $4.0 \times 10^6$ ions per second was delivered to the $8\pi$ spectrometer, in addition to $^{116m2}$In ($I^\pi = 8^-$, $t_{1/2} = 2.18$ s) at $3.2 \times 10^5$ ions per second and $^{116g}$In ($I^\pi = 1^+$, $t_{1/2} = 14.10$ s) at $1.2 \times 10^4$ ions per second. No significant contamination from other species was observed.

The $^{116}$In ions were implanted into a Mylar tape at the center of the $8\pi$ array [13–15], which consists of twenty HPGe detectors, equipped with BGO (bismuth germanate) Compton suppression shields, in a truncated icosahedral arrangement. The $8\pi$ array was augmented with the upstream Pentagonal Array for Conversion Electron Spectroscopy (PACES), consisting of five 5 mm thick lithium-drifted silicon (Si(Li)) detectors for electron detection [16].

Due to the high beam intensity in this experiment, the data acquisition system utilized a complex trigger of scaled-down $\gamma$-ray singles (one event out of every 256 in the trigger logic) and $\gamma$-$\gamma$ coincidences, along with singles events in the PACES Si(Li) array and HPGe-PACES coincidences. The raw data streams were written to disk for offline analysis. Beam cycle times were optimized to observe the $\beta^-$ decay of the $I^\pi = 5^+$ $^{116m1}$In isomer, in which approximately one hour of beam implantation was followed by a one-hour decay, after which the Mylar tape was moved to a Pb-shielded tape box outside the spectrometer. The beam-on and beam-off runs were combined together for the analyses discussed in the present work.

A total of $4 \times 10^9$ HPGe singles events and $4 \times 10^8$ Si(Li) singles events were recorded. The resulting singles spectra are shown in fig. 1 ($\gamma$-ray spectrum), and fig. 2 (conversion electron spectrum). Additionally, several time-random subtracted matrices were created during the offline analysis: a) an unsymmetrized HPGe-PACES matrix containing $2 \times 10^8$ events for $\gamma$-ray and conversion-electron coincidence measurements, and b) symmetrized and unsymmetrized $\gamma$-$\gamma$ matrices, containing coincidence events between pairs of HPGe detectors, used to measure angular correlations and mixing ratios as discussed later.

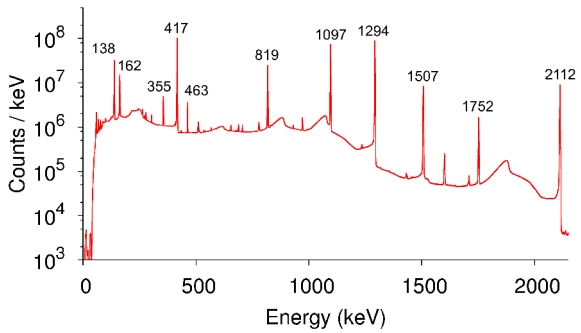


**Fig. 1.** $\gamma$-ray singles spectrum from the $\beta^-$ decay of $^{116}$In with selected transitions labelled with their energies in keV. The 162 keV $\gamma$-ray from the $^{116m2}$In $I^\pi = 8^-$ isomer ($t_{1/2} = 2.18$ s) is present from the beam implantation runs.

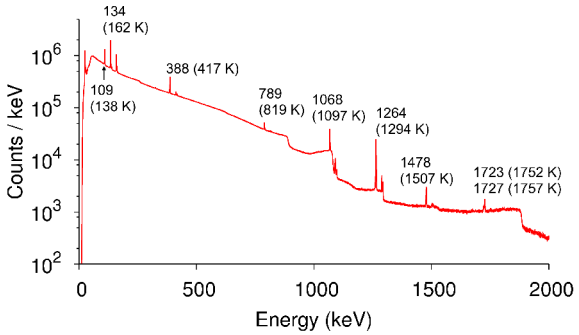


**Fig. 2.** Conversion-electron singles spectrum from the $\beta^-$ decay of $^{116}$In with selected K electron lines labelled with their measured energies and corresponding transition energies in keV.

## 3 Analysis and results

The level scheme of $^{116}$Sn (fig. 3), adapted from the work of Pore *et al.* [17] to include $E0$ transitions either observed in the present work or previously established in the literature, includes transitions examined in this work. The data set analyzed in this work was previously analyzed by Pore *et al.* [17] to report $\gamma$-ray energies, relative intensities, branching ratios, and level energies.

### 3.1 Relative efficiencies

The relative effciency of the $8\pi$ array as a function of energy was measured using standard sealed $^{133}$Ba, $^{152}$Eu, $^{60}$Co, and $^{56}$Co sources. The resulting HPGe relative efficiency curve was then used in constructing the PACES relative efficiency curve.

The efficiency curve for the PACES array, necessary for the conversion-electron analysis and the measurement of K-shell internal conversion coefficients ($\alpha_K$), was obtained through measurements of $\gamma$-ray and electron lines, along with theoretical $\alpha_K$ values, of known transitions in $^{116}$Sn and $^{116m2}$In. The curve was extrapolated to cover the energy range from 50 keV to 2 MeV. In order to specify the PACES efficiency at 71 keV, the $4^+_5 \rightarrow 3^+_1$ and $5^-_1 \rightarrow 3^-_1$

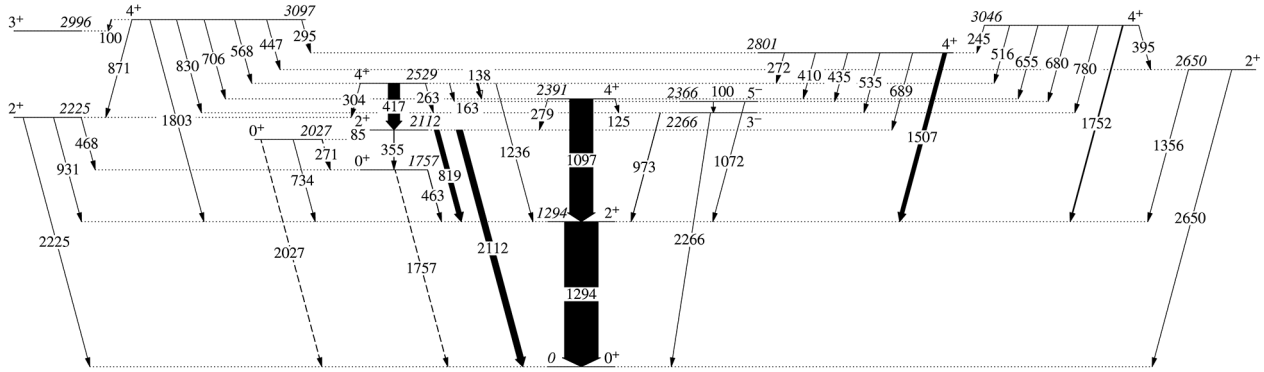


**Fig. 3.** Partial level scheme of $^{116}$Sn adapted from the work of Pore *et al.* [17] on the same data set analyzed in the present work, with arrow widths proportional to $\gamma$-ray relative intensities ($I_\gamma(1294) = 100$). The 271, 1757 and 2027 keV $E0$ transitions (dashed lines) are included for completeness.

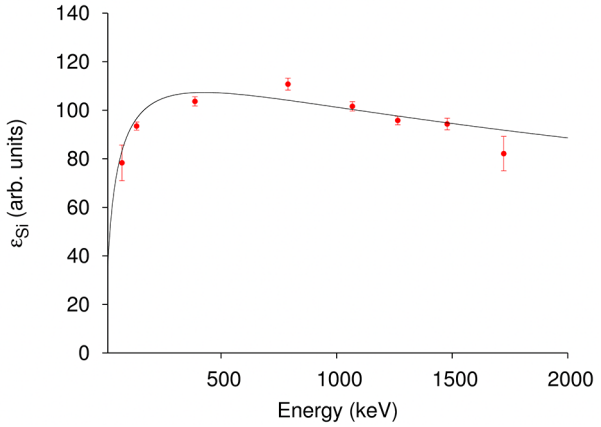


**Fig. 4.** Relative efficiency curve of PACES (solid black line) compared with experimental data points (red dots). A $\chi^2/\nu = 3.02$ was obtained for the fitted curve.

transitions, which overlap at 100 keV, were assumed to be $M1$[1] and $E2$, respectively.

The data points in fig. 4 were obtained using the method developed by Willett [18] to create efficiency curves for Si(Li) detectors when used in conjunction with a $\gamma$-ray detector. The parameterization developed by Willett (adapted from eq. (21) in ref. [18]) to fit efficiencies of Si(Li) detectors was used,

$$\ln(\varepsilon_{Si}) = A[\ln(E)] + B[\ln(E)]^2 - C/E^3 + D, \quad (1)$$

where $E$ is the energy of an electron line in keV. The resulting relative uncertainty in the PACES effciency is $\sim 6\%$.

### 3.2 Conversion-electron data analysis and results

The measured $\alpha_K$ values for several transitions in $^{116}$Sn are summarized in table 1; transitions used to create the efficiency curve have been marked with an asterisk. Comparisons to previous data [1–3,19,20] as well as theoretical $\alpha_K$ calculations from the internal conversion coefficient calculator BrIccFO [21] are also given. The values from ref. [1] are the adopted values listed in the Evaluated Nuclear Structure Data File.

Most of the $\alpha_K$ values in table 1 were obtained from electron and $\gamma$-ray singles measurements using the efficiency-corrected peak areas of K electron lines and their corresponding efficiency-corrected $\gamma$-ray peak areas. However, some were obtained through HPGe-PACES coincidence measurements (marked with a [c] in table 1), normalizing coincidence peak intensities using a similar method developed by Garrett *et al.* [22]. The coincidence gates were necessary to enhance weak electron lines over the high background originating from Compton interactions and $\beta$ particles. Overall, this work confirms previously measured $\alpha_K$ values, and includes new $\alpha_K$ measurements. Most notably, the $2_2^+ \rightarrow 0_3^+$ 85 keV transition connecting the 2112 keV $2_2^+$ state in the proton 2p-2h intruder band to the 2027 keV $0_3^+$ state has been observed, and its $\alpha_K$ was measured to be in reasonable agreement with the theoretical prediction for an $E2$ transition. The observation of the K electron line (fig. 5) confirms the observation of this transition by Pore [17,23] in a $\gamma$-$\gamma$ coincidence analysis.

The measured K/L ratios for selected transitions with visible L lines (*e.g.*, see fig. 6) in $^{116}$Sn and $^{116m2}$In are reported in table 2, and compared to values computed from BrIccFO theoretical $\alpha_{K,L}$ values. These ratios can provide information about the multipolarities of the listed transitions, and thus show that for the transitions used to create the PACES efficiency curve, the chosen $E2$ or $E2/M1$ multipolarities were justified. This also shows that the $4_2^+ \rightarrow 4_1^+$ 138 keV transition is predominantly $M1$. The K/L ratios reported in table 2 are in agreement with previous measurements from the 1960s (refer to the Nuclear Data Sheets [1] and references therein).

Additionally, $\alpha_K$ values, in combination with angular-correlation data, can be used to extract $E0$ components for mixed $E2/M1/E0$ transitions, when the value of $\alpha_K$ is within the $E2$ and $M1$ extreme limits. One such case

[1] Based on the reported $\nu(g_{7/2})$ character of the $3_1^+$ and $4_5^+$ states [10].

**Table 1.** K-shell internal conversion coefficients for transitions in $^{116}$Sn obtained in this work, along with comparisons to previous data. The last two columns show the theoretical $E2$ and $M1$ coefficients from BrIccFO.

| $E_\gamma$ (keV) | $I_i^\pi \to I_f^\pi$ | $\alpha_K$ (ref. [2]) | $\alpha_K$ (ref. [3]) | Lit. $\alpha_K$ (ref. [1])[a] | This work $\alpha_K$ | BrIccFO $E2$ $\alpha_K$ | BrIccFO $M1$ $\alpha_K$ |
|---|---|---|---|---|---|---|---|
| 85 | $2_2^+ \to 0_3^+$ | – | – | –[b] | 2.8(4)[c] | 1.94 | 0.771 |
| 100[d] | $5_1^- \to 3_1^-$ | – | – | 1.4 [19] | 1.40(16)[c] | 1.16 | 0.486 |
| 138 | $4_2^+ \to 4_1^+$ | 0.22(2) | 0.24(2) | 0.26(3) | 0.215(13) | 0.394 | 0.196 |
| 162 ($^{116m2}$In IT)[d] | $8^- \to 5^+$ | – | – | 1.15(9) [20] | 1.05(6)[e] | – | – |
| 304 | $4_2^+ \to 2_3^+$ | – | – | – | 0.026(7)[c] | 0.0286 | 0.0240 |
| 355 | $2_2^+ \to 0_2^+$ | 0.0175(30) | – | 0.018(4) | 0.0171(18)[c] | 0.0174 | 0.0161 |
| 417[d] | $4_2^+ \to 2_2^+$ | 0.0089(8) | 0.0100(10) | 0.0096(10) | 0.0104(6) | 0.0107 | 0.0108 |
| 463 | $0_2^+ \to 2_1^+$ | – | – | – | 0.0070(7)[c] | 0.00788 | 0.00831 |
| 819[d] | $2_2^+ \to 2_1^+$ | 0.0020(2) | 0.0021(2) | 0.0026(3) | 0.00197(12) | 0.00177 | 0.00214 |
| 931 | $2_3^+ \to 2_1^+$ | – | – | 0.00137(4) | 0.0020(8)[c] | 0.00131 | 0.001599 |
| 1097[d] | $4_1^+ \to 2_1^+$ | 0.00099(8) | 0.00100(10) | 0.00094(5) | 0.00093(6) | 0.00091 | 0.001107 |
| 1294[d] | $2_1^+ \to 0_1^+$ | 0.00065(0)[f] | 0.00064(0)[f] | 0.00065(0)[f] | 0.00064(4) | 0.000648 | 0.000772 |
| 1507[d] | $4_3^+ \to 2_1^+$ | 0.00034(3) | 0.00045(7) | 0.00046(3) | 0.00048(3) | 0.000478 | 0.000556 |
| 1752[d] | $4_4^+ \to 2_1^+$ | 0.00053(7) | 0.00031(5) | 0.00038(8) | 0.00032(4) | 0.000358 | 0.000405 |

[a] All values in this column are *verbatim* from ref. [1] unless otherwise indicated.
[b] The only value reported is $\alpha_{tot}$ from a BrIccFO calculation.
[c] Obtained from HPGe-PACES coincidence data.
[d] Transitions used to construct the PACES efficiency curve.
[e] Theoretical $E3$ $\alpha_K = 1.10$.
[f] This value was used to normalize measured $\alpha_K$ values.

is the $4_2^+ \to 4_1^+$ 138 keV transition, discussed in the next section.

## 4 Results from angular correlation measurements

### 4.1 Outline of the theory

Angular correlation measurements in $\beta$-decay experiments usually involve stationary daughter nuclei at room temperature without strong surrounding magnetic fields. Thus, the excited states of the daughter nuclei have randomly oriented angular momentum vectors. The underlying anisotropy of the resulting $\gamma$ radiation is obtained by observing coincident $\gamma$ rays in nuclear cascades in an angular-correlation measurement.

For a cascade of two coincident $\gamma$-rays with spins $I_1 \to I_2 \to I_3$ the angular correlation function $\mathrm{W}(\theta)$ is expressed by

$$\mathrm{W}(\theta) = \mathrm{N}\left[1 + \sum_{k=2,4} \mathrm{A}_{kk}\mathrm{Q}_{kk}\mathrm{P}_k(\cos\theta)\right], \qquad (2)$$

as described in detail in refs. [24–28], where the coefficients $\mathrm{A}_{kk} = \mathrm{B}_k(\gamma_1)\mathrm{A}_k(\gamma_2)$ are the products of the theoretical orientation coefficients $\mathrm{B}_k(\gamma_1)$ and the theoretical directional distribution coefficients $\mathrm{A}_k(\gamma_2)$, the $\mathrm{Q}_{kk}$ factors are the products of attenuation coefficients $\mathrm{Q}_k(\gamma_1)$ and $\mathrm{Q}_k(\gamma_2)$ for detectors of finite size, $\mathrm{P}_k(\cos\theta)$ are the Legendre polynomials, and N is an overall normalization to allow fitting the $\mathrm{W}(\theta)$ function to experimental data.

For mixed $E2/M1$ transitions, the values of $\mathrm{B}_k$ and/or $\mathrm{A}_k$ depend on the mixing ratio $\delta$ [27,28] of the reduced transition matrix elements defined by

$$\delta = \frac{\langle I_{final}\|\hat{M}(E2)\|I_{initial}\rangle}{\langle I_{final}\|\hat{M}(M1)\|I_{initial}\rangle}, \qquad (3)$$

where the sign follows the Krane and Steffen convention [27,28] adopted by the Nuclear Data Sheets [29].

### 4.2 Experimental measurements of angular correlations using the 8$\pi$ array

The HPGe detectors in the 8$\pi$ array can be grouped in four rings of five detectors each. The rings are at 37, 79, 101 and 143 degrees with respect to the beam direction. Pairs of HPGe detectors in the array subtend angles with respect to one another that can be grouped into correlation angles of 41.8, 70.5, 109.5, 138.2, and 180.0 degrees.

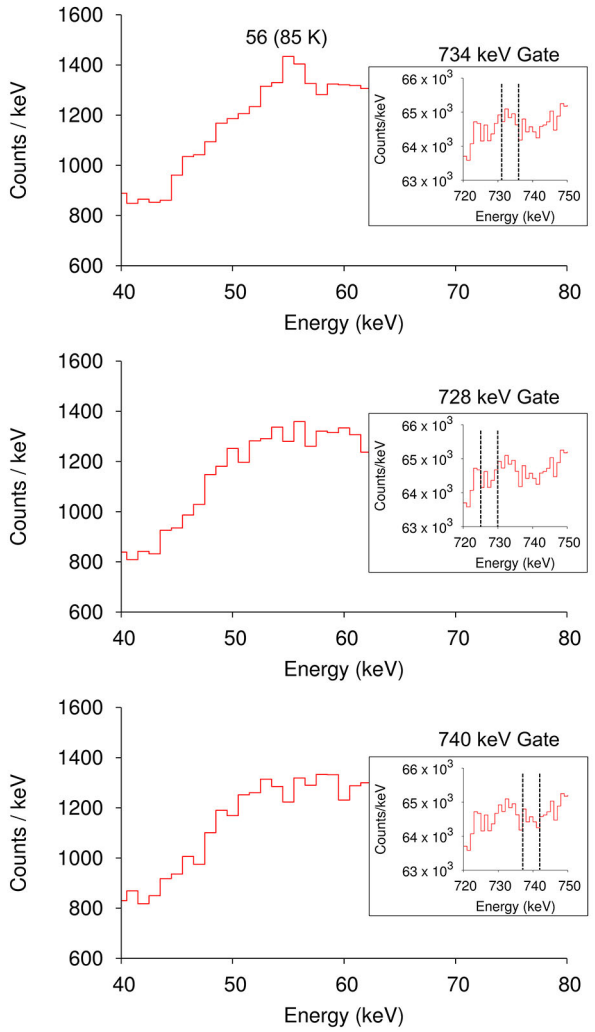


**Fig. 5.** Conversion-electron projections from a gate on 734 keV gamma ray (top) and background to the left (middle) and right (bottom) of the peak showing the emergence of the 85 keV K line at 56 keV only within the gate (note insets which indicate the gate regions for each spectrum).

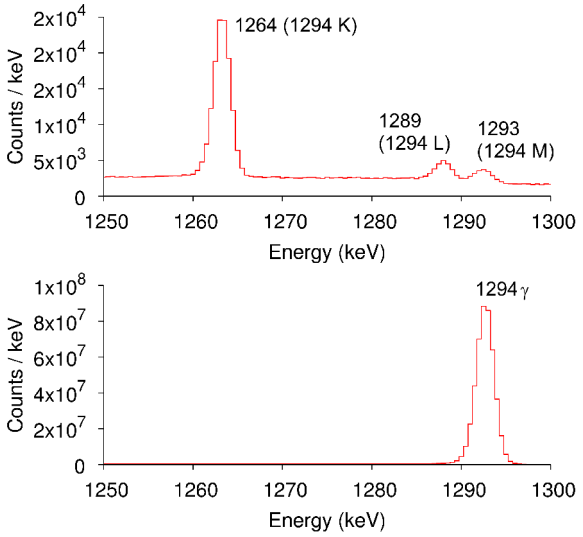


**Fig. 6.** Conversion-electron singles (top) spectrum showing the 1294 keV transition K, L, and M (with possible N, O, ... contributions) electron lines, and the corresponding $\gamma$-ray (bottom) spectrum. Peak energies are labelled in keV.

Coincidences between cascading $\gamma$ rays in pairs of detectors provide the data points which can be fitted with the angular correlation function $W(\theta)$. In the present work, only eighteen of the twenty HPGe detectors were available for angular correlations due to pronounced gain drifts in two detectors. The available number of detector pairs is given in table 3.

The geometric attenuation coefficients $Q_{kk} = Q_k(\gamma_1)$ $Q_k(\gamma_2)$ for the $8\pi$ array of HPGe detectors were computed by Schmelzenbach [30] using a Monte Carlo simulation. These coefficients were found to be relatively insensitive to $\gamma$-ray energy in the range from 100–2000 keV, resulting in $Q_{22} = 0.96$ and $Q_{44} = 0.89$.

To measure angular correlations using the $8\pi$ array, in the offline analysis 153 time-random subtracted $\gamma$-$\gamma$ matrices were created, corresponding to the 153 possible detector pair combinations listed in table 3. Both symmetrized and unsymmetrized (efficiency corrected) matrices were obtained. The creation of the unsymmetrized efficiency-corrected matrices was found to be necessary in order to correct for significant differences in the relative $\gamma$-ray efficiencies of the HPGe detectors at energies below $\sim 500$ keV. The peak areas obtained from coincidence gates in the unsymmetrized efficiency-corrected matrices were normalized by the number of detector pairs in table 3, and then adjusted so that $W(\theta = 180^\circ) = 1$. The underlying statistical errors in the coincident $\gamma$-ray peaks were obtained from the symmetrized matrices, and a 1% systematic uncertainty in the relative $\gamma$-ray efficiency was added in quadrature to each $W(\theta)$ data point.

A first check of the data analysis methodology was to examine the 355–463 keV cascade (2112 keV $(2_2^+) \rightarrow$ 1757 keV $(0_2^+) \rightarrow$ 1294 keV $(2_1^+)$), which should be isotropic with $A_{22} = 0$ and $A_{44} = 0$. The resulting fit yielded $N = 0.998 \pm 0.004$ with $\chi^2/\nu = 0.39$ (fig. 7). Accordingly, for all other angular correlations fitted in this work, a systematic 0.5% normalization relative uncertainty was added, in quadrature, to each $W(\theta)$ data point.

As a further test of the efficiency correction and normalization, angular correlations of pure $E2$ cascades in $^{116}$Sn were fitted with their corresponding theoretical $A_{kk}$ coefficients. For $4^+$-$2^+$-$0^+$ and $0^+$-$2^+$-$0^+$ cascades, $A_{22} = +0.1020$ and $+0.3571$, respectively, and $A_{44} = +0.0091$ and $+1.1429$, respectively.

Two representative pure $E2$ cascades are the 1097–1294 keV cascade (2391 keV $(4_1^+) \rightarrow$ 1294 keV $(2_1^+) \rightarrow$ 0 keV $(0_1^+)$) and the 463–1294 keV cascade (1757 keV $(0_2^+) \rightarrow$ 1294 keV $(2_1^+) \rightarrow$ 0 keV $(0_1^+)$). The theoretical $W(\theta)$ curves using $A_{22}$ and $A_{44}$ coefficients for the associated pure $E2$ cascade type are shown in figs. 8 and 9, respectively, in reasonably good agreement with the data.

**Table 2.** Experimental K/L ratios for transitions in $^{116}$Sn compared to those calculated from BrIccFO. The last column gives the theoretical K/L ratio from BrIccFO; for transitions of mixed multipolarity, mixing ratios measured in the present work were utilized.

| $E_\gamma$ (keV) | $I_i^\pi \rightarrow I_f^\pi$ | This work K/L | BrIccFO K/L |
|---|---|---|---|
| 138 | $4_2^+ \rightarrow 4_1^+$ | 7.8(3) | 7.71 |
| 162 ($^{116m2}$In IT)[a] | $8^- \rightarrow 5^+$ | 2.4(2) | 2.21 |
| 417[a] | $4_2^+ \rightarrow 2_2^+$ | 7.2(2) | 7.11 |
| 819[a] | $2_2^+ \rightarrow 2_1^+$ | 8.0(7) | 8.06 |
| 1097[a] | $4_1^+ \rightarrow 2_1^+$ | 7.9(6) | 8.21 |
| 1294[a] | $2_1^+ \rightarrow 0_1^+$ | 8.6(2) | 8.31 |
| 1507[a] | $4_3^+ \rightarrow 2_1^+$ | 8.5(14) | 8.31 |

[a] Transitions used to construct the PACES efficiency curve.

**Table 3.** List of correlation angles of pairs of detectors in the $8\pi$ array, and the number of detector pairs in each angle.

| Angle number | $\theta$ (degrees) | No. of Detector Pairs |
|---|---|---|
| 1 | 41.8 | 24 |
| 2 | 70.5 | 48 |
| 3 | 109.5 | 48 |
| 4 | 138.2 | 25 |
| 5 | 180.0 | 8 |

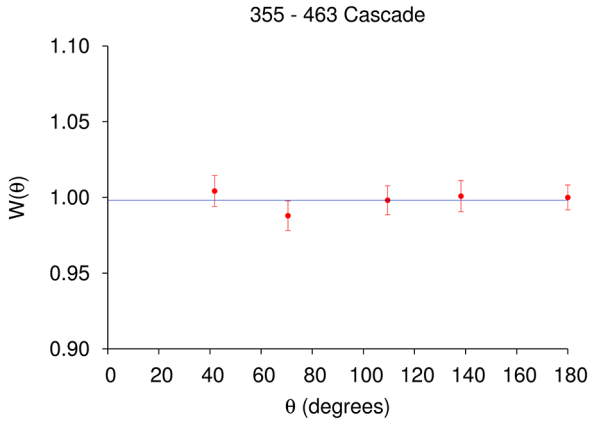


**Fig. 7.** Angular correlation of the $2_2^+$-$0_2^+$-$2_1^+$ 355–463 keV $\gamma$-ray cascade, showing the theoretical fit (blue line) and the data points (red dots, with error bars).

Table 4 summarizes the $\chi^2/\nu$ values obtained for fits to pure $E2$ cascades in $^{116}$Sn with sufficiently intense gamma rays that they can be seen in fig. 1. The relatively large $\chi^2/\nu$ of 5.68 for the 463-1294 cascade is primarily due to the deviation of the W($\theta = 180°$) point from the theoretical curve, and is partly attributable to small discrepancies in the $Q_{kk}$ factors due to slight solid-angle differences in the actual $8\pi$ detector configuration.

### 4.3 Measurements of multipole mixing ratios in $^{116}$Sn

For cascades observed in the decay of the excited $4^+$ and $2^+$ levels, where the decay from the $4^+$ or $2^+$ level under consideration is a mixed $E2/M1$ transition between states of the same spin and parity and the following decay is a pure $E2$ transition, the resulting $A_{22}$ and $A_{44}$ coefficients in eq. (2) are a function of the mixing ratio $\delta$ of the first transition. Therefore, fitting the experimental angular correlation and minimizing $\chi^2/\nu$ as a function of arctan($\delta$) will yield the best value of $\delta$. The mixing ratios

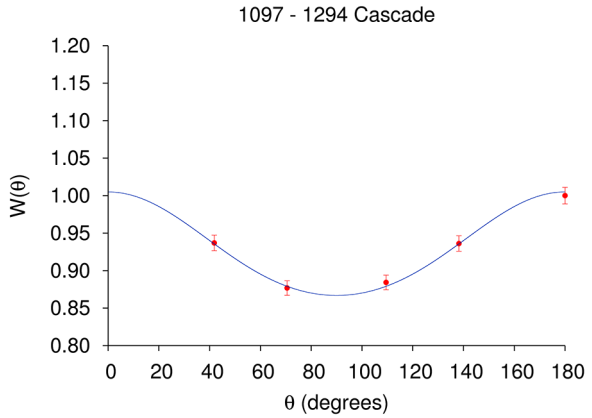


**Fig. 8.** Angular correlation of the $4_1^+$-$2_1^+$-$0_1^+$ 1097–1294 keV $\gamma$-ray cascade. The minimum $\chi^2/\nu$ of this fit is 0.14.

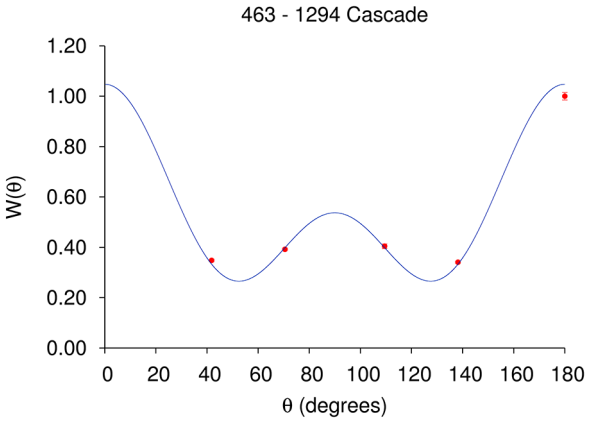


**Fig. 9.** Angular correlation of the $0_2^+$-$2_1^+$-$0_1^+$ 463–1294 keV $\gamma$-ray cascade. The minimum $\chi^2/\nu$ of this fit is 5.68.

**Table 4.** Summary of $\chi^2/\nu$ analyses of fits to pure $E2$ cascades. The second column labels the spins and parities of the states in order of descending level energy, with subscripts indicating the $n$-th occurrence of the state.

| Cascade $\gamma$-rays ($E_\gamma$ in keV) | $I_1^\pi$-$I_2^\pi$-$I_3^\pi$ | $\chi^2/\nu$ |
|---|---|---|
| 463-1294 | $0_2^+$-$2_1^+$-$0_1^+$ | 5.68 |
| 1097-1294 | $4_1^+$-$2_1^+$-$0_1^+$ | 0.14 |
| 1507-1294 | $4_3^+$-$2_1^+$-$0_1^+$ | 0.16 |
| 1752-1294 | $4_4^+$-$2_1^+$-$0_1^+$ | 0.38 |
| 417-355 | $4_2^+$-$2_2^+$-$0_2^+$ | 0.51 |
| 417-2112 | $4_2^+$-$2_2^+$-$0_1^+$ | 0.08 |

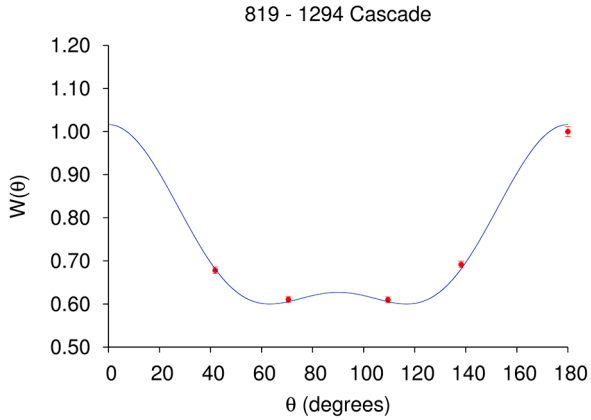


**Fig. 10.** Angular correlation of the $2_2^+ \rightarrow 2_1^+ \rightarrow 0_1^+$ 819–1294 keV $\gamma$-ray cascade. The minimum $\chi^2/\nu$ of this fit is 1.43.

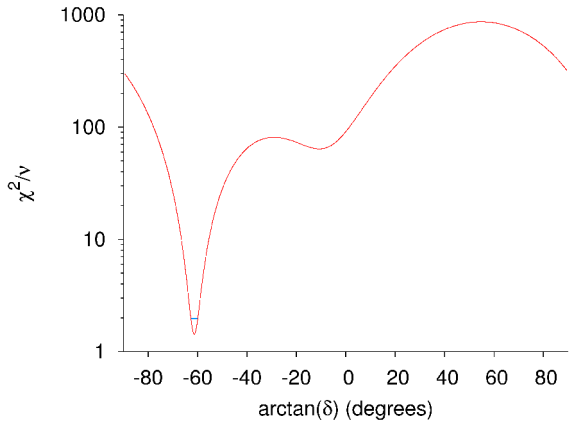


**Fig. 11.** Plot of $\chi^2/\nu$ as a function of arctan($\delta$) in degrees for the 819–1294 keV $\gamma$-ray cascade. The blue bar indicates the uncertainty in the value of $\delta$, determined at the limits of the unreduced $\chi^2$(min) + 1.

for transitions between several excited $2^+$ and $4^+$ levels populated in $^{116}$Sn are summarized in table 5; selected transitions will be discussed in more detail below.

The 819–1294 keV cascade (2112 keV ($2_2^+$) $\rightarrow$ 1294 keV ($2_1^+$) $\rightarrow$ 0 keV ($0_1^+$)), serves as a useful benchmark for the mixing ratio measurements in the present work. The

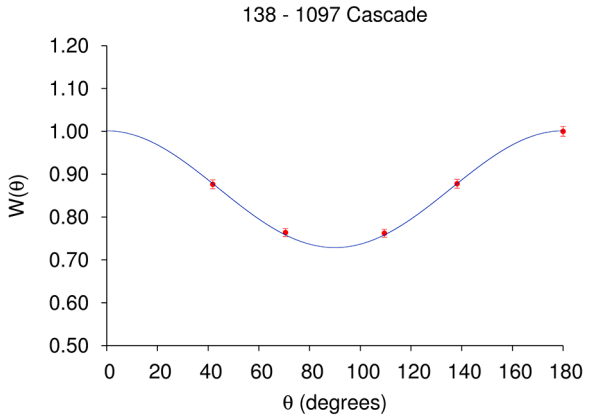


**Fig. 12.** Angular correlation of the $4_2^+ \rightarrow 4_1^+ \rightarrow 2_1^+$ 138–1097 keV $\gamma$-ray cascade. The minimum $\chi^2/\nu$ of this fit is 0.10.

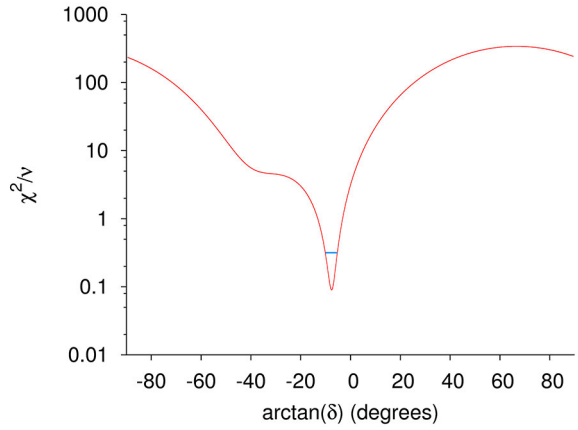


**Fig. 13.** Plot of $\chi^2/\nu$ as a function of arctan($\delta$) in degrees for the 138–1097 keV $\gamma$-ray cascade. The blue bar indicates the uncertainty in the value of $\delta$, determined at the limits of the unreduced $\chi^2$(min) + 1.

1294 keV transition is a pure $E2$ transition. The $2_2^+ \rightarrow 2_1^+$ 819 keV transition, however, has previously been established to be a mixed $E2/M1$ transition, with $\delta = -1.8(2)$ [1]. In the present work, the $\chi^2/\nu$ minimization analysis of the 819-1294 cascade (figs. 10 and 11) yielded $\delta = -1.83(8)$, in good agreement with the previously reported literature value.

The $4_2^+ \rightarrow 4_1^+$ 138 keV transition, part of the 138–1097 keV cascade (2529 keV ($4_2^+$) $\rightarrow$ 2391 keV ($4_1^+$) $\rightarrow$ 1294 keV ($2_1^+$)) has only been studied once previously in an angular correlation measurement; the values $A_{22} = 0.20(7)$ and $A_{44} = -0.10(11)$ were reported by Bron *et al.* [5], but no $\delta$ value was reported. In the present work, the $\delta$ of this transition was measured to be $-0.13(8)$, (figs. 12 and 13), consistent with the measured K/L ratio in table 2, indicating a nearly pure $M1$ transition with $1.7^{+2.6}_{-1.4}$% $E2$ character. From the mixing ratio determined in the present work together with $t_{1/2} < 100$ ps for the 2529 keV state [1], the new limits of $B(M1) > 0.0092$ W.u., $B(E2) > 0.95$ W.u., are obtained for this transition.

**Table 5.** Summary of results of angular correlation measurements of mixed-multipole transitions in $^{116}$Sn. The spins and parities in the third column are in order of descending level energy. The sign of $\delta$ uses the Krane and Steffen convention [27,28].

| Cascade $\gamma$ rays ($E_\gamma$ in keV) | Originating level energy (keV) | $I_1^\pi$-$I_2^\pi$-$I_3^\pi$ | $\delta$ | $\chi^2/\nu$ |
|---|---|---|---|---|
| 272-417 | 2801 | $4_3^+$-$4_2^+$-$2_2^+$ | $-0.9^{+1.0}_{-0.4}$ | 1.58 |
| 568-417 | 3097 | $4_5^+$-$4_2^+$-$2_2^+$ | $-0.9^{+1.0}_{-0.4}$ | 0.40 |
| 138-1097 | 2529 | $4_2^+$-$4_1^+$-$2_1^+$ | $-0.13(8)$ | 0.10 |
| 410-1097 | 2801 | $4_3^+$-$4_1^+$-$2_1^+$ | $-0.2^{+0.2}_{-0.5}$ | 0.52 |
| 655-1097 | 3046 | $4_4^+$-$4_1^+$-$2_1^+$ | $+0.26^{+0.20}_{-0.20}$ | 0.55 |
| 706-1097 | 3097 | $4_5^+$-$4_1^+$-$2_1^+$ | $-0.13^{+0.12}_{-0.18}$ | 0.71 |
| 819-1294 | 2112 | $2_2^+$-$2_1^+$-$0_1^+$ | $-1.83(8)$ | 1.43 |
| 931-1294 | 2225 | $2_3^+$-$2_1^+$-$0_1^+$ | $+1.8^{+0.7}_{-0.5}$ | 1.87 |
| 245-1507 | 3046 | $4_4^+$-$4_3^+$-$2_1^+$ | $-0.9(5)$ | 0.34 |

If the 138 keV transition were pure $M1$, the theoretical BrIccFO internal conversion coefficient would be $\alpha_K = 0.196$. Previous experimental values of $\alpha_K$ for this transition (see table 1) are greater than 0.2, similar to the $\alpha_K$ obtained in the present work of 0.215(13). In a similar analysis to that for the 819 keV transition examined by Yamaguchi *et al.* [3], an $E0$ component may be present in the 138 keV transition. An indirect measurement of the $E0$ component in a mixed transition can be obtained from the following relationship, adapted from ref. [3], namely

$$\alpha_K(\text{exp}) = \frac{(\mu_K + \alpha_K(E2))\delta^2 + \alpha_K(M1)}{1+\delta^2}, \qquad (4)$$

where the ratio $\mu_K$ is defined as the $E0$ component of the K line intensity divided by the $E2$ component of the corresponding $\gamma$-ray intensity, and $\alpha_K(E2)$ and $\alpha_K(M1)$ are the theoretical values obtained from BrIccFO. In this work we obtain $\mu_K = 0.9^{+6.5}_{-0.9}$ for the 138 keV transition. The dimensionless ratio $X = B(E0)/B(E2)$ [31] can then be obtained from $\mu_K$, yielding $X = 0.05^{+0.34}_{-0.05}$. The central value of $X$ corresponds to an absolute $B(E2) = 6.37$ W.u. (obtained from $\delta = -0.13$), which results in a deduced $E0$ strength of $\rho^2(E0) \times 10^3 = 9.0^{+1.6}_{-9.0}$. The upper $\rho^2(E0)$ limit is consistent with the $B(E2)$ limit of 0.95 W.u..

In principle, it is also possible to find $E0$ components for other transitions between states of the same spin and parity in $^{116}$Sn, but the required $\alpha_K$ values cannot be obtained in coincidence gates with sufficient statistics, and the associated mixing ratios have somewhat large uncertainties. Two exceptions, which have been re-measured in the present work, are the $2_2^+ \rightarrow 2_1^+$ 819 keV and the $2_3^+ \rightarrow 2_1^+$ 931 keV transitions, utilizing the $\alpha_K$ values from table 1 and the mixing ratios from table 5. The corresponding $\mu_K$ values show negligible $E0$ components for both, with $\mu_K(819) < 2.2 \times 10^{-4}$ and $\mu_K(931) < 1.8 \times 10^{-3}$.

The mixing ratio of the $2_3^+ \rightarrow 2_1^+$ 931 keV transition was measured previously by Kantele *et al.* [32] as $-1.9^{+0.5}_{-0.7}$, in the Krane and Steffen convention. However, the reported sign is incorrect; given the reported values of $A_{22} = -0.31(2)$ and $A_{44} = +0.37(4)$, the central value of $\delta$ should have been +1.9, consistent with the value of $\delta = +1.8^{+0.7}_{-0.5}$ obtained in the present work. The positive sign of $\delta$ was also confirmed in a recent measurement by Urban *et al.* [33], who reported $\delta = +3.44(40)$, but the magnitude of $\delta$ disagrees with both the values obtained in the present work and by Kantele *et al.* [32].

## 5 Discussion

The comprehensive review of the level energies in $^{116}$Sn below 4.3 MeV by Raman *et al.* [34] characterized them in terms of proton 2p-2h excitations, phonon states, and broken-pair states. Other spectroscopic data, such as transition probabilities or mixing ratios, were not discussed when assigning the character of the states. The data obtained in the present analysis will be used to re-examine the low-lying $2_2^+$, $2_3^+$ and $4_{1-5}^+$ states in $^{116}$Sn, taking into account the measured mixing ratios as well as deduced relative transition strengths.

### 5.1 The 2112 keV $2_2^+$ and 2225 keV $2_3^+$ levels

The 2112 keV $2_2^+$ level is well-characterized as containing mostly proton 2p-2h quasi-rotational character [34], supported by the results of the $(p,p')$ experiment conducted by Wienke *et al.* [7]. In a $(d,p)$ one-neutron transfer experiment, Schneid *et al.* [8] did not report any population of this state, also consistent with a dominant proton 2p-2h assignment.

The characterization of the 2225 keV $2_3^+$ level is less clear, as Wienke *et al.* could not explain the $(p,p')$ angular distribution through assigning two-phonon character to this state. Schneid *et al.* reported a spin-weighted spectroscopic strength of $S' = 0.98$ for this state in the $(d,p)$ reaction [8], indicating an almost pure shell-model neutron state, dominated by either $\nu(s_{1/2}, d_{3/2})$ or $\nu(s_{1/2}, d_{5/2})$ configurations [35,10]. The neutron configuration is supported by the preferred $\beta^+$/EC decay of the $[\pi(d_{5/2}) \otimes \nu(s_{1/2})]3^+$ $^{116}$Sb ground state to the

**Table 6.** Relative $B(M1)$ values for selected transitions in $^{116}$Sn, based on $\gamma$-ray intensities from Pore *et al.* [17] and mixing ratios from this work. The largest relative $B(M1)$ exiting each level is normalized to 100. Transitions marked with the letter $^a$ are assumed to be pure $M1$. The 51 keV $\gamma$ ray, noted in parentheses, was not observed in the present work but is included for completeness.

| $E_{level}$ (keV) | $E_\gamma$ (keV) | $I_\gamma$ | $I^\pi_{initial}$ | $I^\pi_{final}$ | Relative $B(M1)$ value |
|---|---|---|---|---|---|
| 2529 | 138 | 4.63(11) | $4^+_2$ | $4^+_1$ | $100^{+2}_{-3}$ |
| 2801 | 410 | 0.0735(26) | $4^+_3$ | $4^+_1$ | $96^{+3}_{-25}$ |
| | 272 | 0.0405(13) | | $4^+_2$ | $100^{+87}_{-35}$ |
| 3046 | 655 | 0.141(4) | $4^+_4$ | $4^+_1$ | $34^{+2}_{-4}$ |
| | 516$^a$ | 0.0189(18) | | $4^+_2$ | $10^{+1}_{-1}$ |
| | 245 | 0.0360(12) | | $4^+_3$ | $100^{+57}_{-36}$ |
| 3097 | 706 | 0.187(5) | $4^+_5$ | $4^+_1$ | $100^{+2}_{-7}$ |
| | 568 | 0.0522(21) | | $4^+_2$ | $31^{+23}_{-10}$ |
| | 295$^a$ | 0.00750(66) | | $4^+_3$ | $56^{+5}_{-5}$ |
| | (51) | – | | $4^+_4$ | – |

2225 keV $2^+_3$ level ($\log ft = 4.78$, as compared to 6.79 for the 2112 keV level [1]). The 2225 keV level thus cannot be interpreted as a two-phonon vibrational state, in contrast to the assignment by Raman *et al.* [34].

The 2112 keV $2^+_2$ and 2225 keV $2^+_3$ levels decay to the 1294 keV $2^+_1$ level through 819 and 931 keV transitions, respectively, which have opposite signs for their mixing ratios as shown in table 5. This is consistent with the differing character of the initial states. Furthermore, the absence of the $2^+_3 \rightarrow 2^+_2$ 113 keV transition supports the lack of mixing between these states.

### 5.2 The 2391, 2529, 2801, 3046 and 3097 keV $4^+$ levels

The very similar allowed $\log ft$ values of $\sim 5.2$ [1] for $\beta^-$ decay from the $^{116m1}$In $[\pi(g_{9/2})^{-1} \otimes \nu(s_{1/2})]5^+$ isomer to the $4^+$ states below 3.4 MeV in $^{116}$Sn suggests that they all share a one broken pair $\nu(g_{7/2})^{-1}(s_{1/2})$ configuration. Supporting the suggestion of a high degree of mixing is the reported fragmentation of the $L = 4$ hexadecapole strength in the $(p, p')$ experiment by Wienke *et al.* [7], indicating an excitation of a neutron between the $\nu(g_{7/2})$ and the $\nu(s_{1/2})$ orbitals. Nevertheless, the analysis by Raman *et al.* [34] excluded the 2529 keV $4^+_2$ state from this group, assigning it pure proton 2p-2h character (which can be supported from the experiments performed by Bron *et al.* [5] and Poelgeest *et al.* [35]).

To further probe the character of the $4^+_{1-5}$ states through their decay patterns, the measured mixing ratios in table 5 combined with the $\gamma$-ray intensities reported by Pore *et al.* [17] have been used to compute relative $B(M1; 4^+ \rightarrow 4^+)$ values (table 6). In addition, relative $B(E2; 4^+ \rightarrow 2^+)$ values are shown in table 7. It should be noted that *quantitative* comparisons of relative strengths are only strictly applicable when comparing transitions exiting the same state.

The relative $M1$ strengths in table 6 and relative $E2$ strengths in table 7, utilizing $\gamma$-ray intensity data from Pore *et al.* [17], measure relative transition probabilities to lower-lying levels such that the strongest transition de-exciting a given level is normalized to 100. In comparing relative $M1$ strengths to relative $E2$ strengths, it can be seen that the relative $M1$ strengths for branches within a given level differ at most by a factor of $\sim 10$. In contrast, the relative $E2$ strengths show more variation; in some cases, one transition tends to dominate over the others for de-excitations from a given level.

The high degree of mixing of the $4^+_{1-5}$ states is consistent with relative $M1$ strengths which do not exhibit a strongly preferential decay to only one lower-lying level. Since the low-lying $2^+$ states have different wavefunction constituents, the relative $E2$ strengths can indicate how the higher-lying $4^+_{1-5}$ states differ from one another.

The newly-measured $E0$ component of the $4^+_2 \rightarrow 4^+_1$ 138 keV transition may suggest shape coexistence of the 2529 keV $4^+_2$ (considered to be pure proton 2p-2h [34]) and the 2391 keV $4^+_1$ (considered to be predominantly neutron broken-pair [34]) states as part of their intruder-yrast mixing. Reinforcing this, the 2801 keV $4^+_3$ state decays to the $4^+_2$ and $4^+_1$ states with approximately equal central values of relative $M1$ strengths, differing at most by a factor of $\sim 2$. The relative $E2$ strengths for the 689 and 1507 keV transitions to the 2112 keV $2^+_2$ (2p-2h) and 1294 keV $2^+_1$ (yrast) states are very similar in magnitude, as well. Furthermore, the 3033 keV $6^+_1$ state in the proton 2p-2h intruder band has not been observed to

**Table 7.** Relative $B(E2)$ values for selected transitions in $^{116}$Sn, based on $\gamma$-ray intensities from Pore *et al.* [17]. The largest relative $B(E2)$ exiting each level is normalized to 100. Gamma rays in parentheses were not observed in the present work, but are included to show the differences in the decay patterns.

| $E_{level}$ (keV) | $E_\gamma$ (keV) | $I_\gamma$ | $I^\pi_{initial}$ | $I^\pi_{final}$ | Relative $B(E2)$ value |
|---|---|---|---|---|---|
| 2391 | 1097 | 69.2(8) | $4^+_1$ | $2^+_1$ | 42.2(5) |
| | 279 | 0.158(5) | | $2^+_2$ | 91(3) |
| | 165 | $< 0.013$ | | $2^+_3$ | $< 100$ |
| 2529 | 1236 | 0.0683(36) | $4^+_2$ | $2^+_1$ | 0.00089(5) |
| | 417 | 33.7(10) | | $2^+_2$ | 100(3) |
| | 304 | 0.142(3) | | $2^+_3$ | 2.05(4) |
| 2801 | 1507 | 11.7(3) | $4^+_3$ | $2^+_1$ | 100(3) |
| | 689 | 0.208(7) | | $2^+_2$ | 90(3) |
| | (576) | – | | $2^+_3$ | – |
| | (151) | – | | $2^+_4$ | – |
| 3046 | 1752 | 2.79(7) | $4^+_4$ | $2^+_1$ | 26.4(7) |
| | (934) | – | | $2^+_2$ | – |
| | (821) | – | | $2^+_3$ | – |
| | 395 | 0.00620(33) | | $2^+_4$ | 100(5) |
| 3097 | 1803 | $< 0.00545$ | $4^+_5$ | $2^+_1$ | $< 0.333$ |
| | (985) | – | | $2^+_2$ | – |
| | 871 | 0.00609(44) | | $2^+_3$ | 14(1) |
| | 447 | 0.00153(15) | | $2^+_4$ | 100(10) |

decay to the 2801 keV $4^+_3$ state [5], suggesting that the $4^+_3$ state is pure neutron broken-pair in nature. These all combine to suggest that the 2529 keV $4^+_2$ state must contain a $\nu(g_{7/2})^{-1}(s_{1/2})$ component, in contrast to Raman *et al.* [34] interpreting it as a pure proton 2p-2h state.

The extent of the $E0$ mixing contribution to the intruder-yrast mixing of the $4^+_{1,2}$ states can be determined, in analogy to the $0^+$ two-state configuration mixing model set forth by Wood *et al.* [36]. We start by expressing the $4^+_1$ and $4^+_2$ wavefunctions as follows, in terms of a mixing parameter $a$:

$$|4^+_1\rangle = a\,|4^+_{intruder}\rangle + \sqrt{1-a^2}\,|4^+_{yrast}\rangle\,, \quad (5)$$

$$|4^+_2\rangle = -\sqrt{1-a^2}\,|4^+_{intruder}\rangle + a\,|4^+_{yrast}\rangle\,. \quad (6)$$

The corresponding $\rho^2(E0)$ can be obtained from eq. (51) of ref. [36], namely

$$\rho^2(E0) = \left(\frac{3}{4\pi}Z\right)^2 a^2(1-a^2)\left[\Delta(\beta^2)\right]^2\,, \quad (7)$$

where $\Delta(\beta^2) = \beta^2(\text{intruder}) - \beta^2(\text{yrast})$. Assuming that the deformations obtained from the respective $2^+ \to 0^+$ transitions in the intruder and yrast bands are negligibly changed for the $4^+$ members of each band, then $\beta = 0.1118(16)$ for the 2391 keV state [37] (also consistent with the measurement by Wienke *et al.* [7]). For the 2529 keV state, $\beta = 0.209(8)$ based on the $B(E2)$ value for the 355 keV transition [17] (also see similar results given by refs. [38,39]).

We find from the limits on $\rho^2(E0)$ that $a^2 = 0.070^{+0.014}_{-0.070}$, suggesting weaker mixing than that deduced by Pore *et al.* [17]. However, this treatment only analyzes the $E0$ mixing portion of the overall intruder-yrast mixing, as opposed to deducing the overall mixing from the rotational parameters in the intruder band. In addition, if the $\beta$ for the yrast $4^+_1$ state is correlated with the rise in the in-band $B(E2)$ strength (such that $\beta$ might be $\approx 0.14$ instead of $\approx 0.11$), the value of $a^2$ would increase due to the greater similarity of the shapes.

Finally, Pore *et al.* [17] suggested that the half-life of the 2529 keV $4^+_2$ state could be as low as 10 ps. Correspondingly, the $E0$ strength would rise by approximately

the same factor of 10, implying maximal mixing of the states. In fact, for the deformations given above, maximal mixing would occur at $\rho^2(E0) \times 10^3 \approx 35$. Thus, the 2529 keV $4_2^+$ state could be more deformed than assumed in the above analysis, but further work is clearly necessary to better probe the $E0$ and non-$E0$ mixing between the $4_2^+$ and $4_1^+$ states.

The 3046 keV $4_4^+$ and 3097 keV $4_5^+$ states preferentially decay into the 2650 keV $2_4^+$ state, and exhibit comparatively smaller $E2$ strength into other low-lying $2^+$ states. The 2650 keV state, suggested to contain a large $\nu(\mathrm{d}_{5/2})^2$ component [10], primarily feeds the $2_1^+$ state and the $0_1^+$ ground state. The difference in the $E2$ decay character of the $4_{4,5}^+$ states, compared to the lower-lying $4_{1-3}^+$ states, suggests that the $4_4^+$ state contains admixtures of $\nu(\mathrm{d}_{3/2})$ and $\nu(\mathrm{d}_{5/2})$ components, while the $4_5^+$ state contains predominantly a $\nu(\mathrm{d}_{5/2})^2$ admixture in addition to the common $\nu(\mathrm{g}_{7/2})^{-1}(\mathrm{s}_{1/2})$ component across all the $4_{1-5}^+$ states.

In summary, the relative $E2$ and $M1$ transition probabilities computed in the present work confirm the mixing of the $4_{1-5}^+$ states. In particular, the relative transition probabilties for the decays of the 2801 keV $4_3^+$ state, a pure neutron broken-pair state, suggest that the 2529 keV $4_2^+$ state contains a neutron broken-pair admixture to its dominant proton 2p-2h component.

## 6 Conclusion

A high-statistics $\beta$-decay experiment involving the decay of $^{116m1}$In to $^{116}$Sn using the $8\pi$ spectrometer at TRIUMF-ISAC has provided a robust data set which has given rise to several new measurements of K-shell internal conversion coefficients, $E2/M1$ mixing ratios and relative transition probabilities. While the measured mixing ratios are in several cases statistics-limited, they do shed light on the configuration mixing of the $2^+$ and $4^+$ states, enabling a better understanding of the nature of the excited states of $^{116}$Sn. However, absolute $B(E2)$ and $B(M1)$ values determined from lifetime data are required to better understand the underlying wavefunction admixtures of the low-lying $4^+$ states in $^{116}$Sn.

We wish to thank T. Drake for helpful commentary and discussions regarding aspects of the analysis of the $^{116}$Sn data. Funding for this research was provided by the Natural Sciences and Engineering Research Council and by the U.S. National Science Foundation under grant number PHY-1606890. TRIUMF receives federal funding via a contribution agreement through the National Research Council of Canada.

## References

1. J. Blachot, Nucl. Data Sheets **111**, 717 (2010).
2. F. Pleiter, Nucl. Phys. A **184**, 443 (1972).
3. Y. Yamaguchi, J. Runan(Gen), T. Nagahara, J. Phys. Soc. Jpn. **38**, 911 (1975).
4. K.S. Krane, J. Sylvester, Phys. Rev. C **054312**, 73 (2006).
5. J. Bron *et al.*, Nucl. Phys. A **318**, 335 (1979).
6. A. Savelius *et al.*, Nucl. Phys. A **637**, 491 (1998).
7. H. Wienke, H.P. Blok, J. Blok, Nucl. Phys. A **405**, 237 (1983).
8. E.J. Schneid, A. Prakash, B.L. Cohen, Phys. Rev. **156**, 1316 (1967).
9. H.W. Fielding *et al.*, Nucl. Phys. A **281**, 389 (1977).
10. J.M. Schippers *et al.*, Nucl. Phys. A **510**, 70 (1990).
11. E.R. Flynn, P.D. Kunz, Phys. Lett. B **68**, 40 (1977).
12. G. Wenes *et al.*, Phys. Rev. C **23**, 2291 (1981).
13. G.C. Ball *et al.*, J. Phys. G: Nucl. Part. Phys. **31**, S1491 (2005).
14. A.B. Garnsworthy, C.E. Svensson, Hyperfine Interact. **225**, 127 (2013).
15. P.E. Garrett *et al.*, J. Phys. G Conf. Ser. **639**, 012006 (2015).
16. E.F. Zganjar *et al.*, Acta Phys. Pol. B **38**, 1179 (2007).
17. J.L. Pore *et al.*, Eur. Phys. J. A **53**, 27 (2017).
18. J.B. Willett, Nucl. Instrum. Methods **84**, 157 (1970).
19. B. Skytte Jensen, O.B. Nielsen, O. Skilbreid, Nucl. Phys. **19**, 654 (1960).
20. P.H. Heckmann, K. Gubenator, J. Poyhonen, A. Flammersfeld, Z. Phys. **163**, 451 (1961).
21. T. Kibédi, T.W. Burrows, M.B. Trzhaskovskaya, P.M. Davidson, C.W. Nestor Jr., Nucl. Instrum. Methods A **589**, 202 (2008).
22. P.E. Garrett *et al.*, EPJ Web of Conferences **123**, 02005 (2016).
23. J.L. Pore, MSc Thesis, Simon Fraser University (2013).
24. D.R. Hamilton, Phys. Rev. **58**, 122 (1940).
25. L.C. Biedenharn, M.E. Rose, Rev. Mod. Phys. **25**, 729 (1953).
26. H.J. Rose, D.M. Brink, Rev. Mod. Phys. **39**, 306 (1967).
27. A.J. Becker, R.M. Steffen, Phys. Rev. **180**, 1043 (1969).
28. K.S. Krane, R.M. Steffen, Phys. Rev. C **2**, 724 (1970).
29. J.K. Tuli, private communication.
30. P. Schmelzenbach, PhD Thesis, Oregon State University (2003).
31. T. Kibédi *et al.*, Nucl. Phys. A **688**, 669 (2001).
32. J. Kantele *et al.*, Z. Phys. A **289**, 157 (1979).
33. W. Urban *et al.*, JINST **8**, P03014 (2013).
34. S. Raman *et al.*, Phys. Rev. C **43**, 521 (1991).
35. A. van Poelgeest *et al.*, Nucl. Phys. A **346**, 70 (1980).
36. J.L. Wood, E.F. Zganjar, C. De Coster, K. Heyde, Nucl. Phys. A **651**, 323 (1999).
37. S. Raman, C.W. Nestor, P. Tikkanen, At. Data Nucl. Data Tables **78**, 1 (2001).
38. A. Bäcklin *et al.*, Nucl. Phys. A **351**, 490 (1981).
39. N.G. Jonsson *et al.*, Nucl. Phys. A **371**, 333 (1981).